Pharmacological inhibitor of DNA-PK, M3814, potentiates radiotherapy and regresses human tumors in mouse models

Authors:

Frank T. Zenke[1], Astrid Zimmermann[1], Christian Sirrenberg[1], Heike Dahmen[1], Vladimir Kirkin[2], Ulrich Pehl[3], Thomas Grombacher[4], Claudia Wilm[1], Thomas Fuchss[3], Christiane Amendt[1], Lyubomir T. Vassilev[5], Andree Blaukat[1]

Affiliations:

[1]Merck KGaA, Biopharma R&D, Translational Innovation Platform Oncology, Frankfurter Str. 250, 64293 Darmstadt, Germany; [2]The Institute of Cancer Research, Cancer Research UK Cancer Therapeutics Unit, 15 Cotswold Road, Sutton, London, SM2 5NG, UK; [3]Merck KGaA, Biopharma R&D, Discovery Development Technologies, Frankfurter Str. 250, 64293 Darmstadt, Germany; [4]Merck KGaA, Biopharma R&D, Translational Medicine, Frankfurter Str. 250, 64293 Darmstadt, Germany; [5]EMD Serono Research and Development Institute Inc., Biopharma R&D, Translational Innovation Platform Oncology, 45A Middlesex Turnpike, Billerica, MA 01821-3936, USA; a business of Merck KGaA, Darmstadt, Germany

Email addresses:

frank.zenke@merckgroup.com

astrid.zimmermann@merckgroup.com

christian.sirrenberg@merckgroup.com

heike.dahmen@merckgroup.com

vladimir.kirkin@icr.ac.uk

ulrich.pehl@merckgroup.com

thomas.grombacher@merckgroup.com

claudia.wilm@merckgroup.com

thomas.fuchss@merckgroup.com

christiane.amendt@merckgroup.com

lubo.vassilev@emdserono.com

andree.blaukat@merckgroup.com

Running title: Preclinical pharmacology of M3814 in cancer models

Suggested keywords (max 5): Non-homologous end joining; DNA-damage repair; DNA-dependent protein kinase; ionizing radiation; M3814

Additional information:

Financial support: This work was funded by Merck KGaA, Darmstadt, Germany

Corresponding author: Frank T. Zenke; Merck KGaA, Frankfurter Str. 250, 64293 Darmstadt, Germany; email: frank.zenke@merckgroup.com; Tel: +49 (0)6151 72-4730; Fax: +49 (0)6151 72-7398.

Conflict of interest disclosure statement:

All authors are employees of Merck KGaA or EMD Serono, except for Vladimir Kirkin, who is a former employee of Merck KGaA.

Word count: 4605/5000 (includes Introduction, Results, Discussion, Acknowledgements, Figure legends)

Figures/tables: 6/6

Abstract (214/250 words)

Physical and chemical DNA-damaging agents are used widely in the treatment of cancer. Double-strand break (DSB) lesions in DNA are the most deleterious form of damage and, if left unrepaired, can effectively kill cancer cells. DNA-dependent protein kinase (DNA-PK) is a critical component of non-homologous end joining (NHEJ), one of the two major pathways for DSB repair. Whilst DNA-PK has been considered an attractive target for cancer therapy, the development of pharmacological DNA-PK inhibitors for clinical use has been lagging. Here, we report the discovery and characterization of a potent, selective, and orally bioavailable DNA-PK inhibitor, M3814, and provide in vivo proof of principle for DNA-PK inhibition as a novel approach to combination radiotherapy. M3814 potently inhibits DNA-PK catalytic activity and sensitizes multiple cancer cell lines to ionizing radiation (IR) and DSB-inducing agents. Inhibition of DNA-PK autophosphorylation in cancer cells or xenograft tumors led to an increased number of persistent DSBs. Oral administration of M3814 to two xenograft models of human cancer, using a clinically established 6-week fractionated radiation schedule, strongly potentiated the antitumor activity of IR and led to complete tumor regression at non-toxic doses. Our results strongly support DNA-PK inhibition as a novel approach for the combination radiotherapy of cancer. M3814 is currently under investigation in combination with radiotherapy in clinical trials.

Introduction

To ensure the accurate maintenance and transfer of genetic information to progeny, mammalian cells have evolved sophisticated mechanisms to sense DNA damage, coordinate its repair, and prevent potential tumorigenic effects; this is collectively known as the DNA damage response (DDR). Defects in the DDR contribute to genomic instability and represent one of the key hallmarks of cancer (1). DNA can be damaged by multiple endogenous and exogenous factors. Many established therapeutic modalities, such as radio- and chemotherapy that attack cancer cell DNA are in clinical use but provide limited benefit to cancer patients. This is due, at least in part, to the competence of tumor cells to deal with DNA damage (2).

Diverse types of lesions can be generated in DNA, ranging from base modifications to strand breaks, leading to large deletions or genomic rearrangements. Of those, double-strand breaks (DSBs) are considered the most harmful and can have lethal consequences for the cells and organism if left unrepaired (3). DSB repair is accomplished through two major pathways, homologous recombination-guided repair (HR) and non-homologous end joining (NHEJ) (3,4). HR requires an intact DNA strand as a template for break repair and is restricted to the S and G2 phases of the cell cycle. Therefore, HR is considered less error prone than NHEJ. Conversely, NHEJ repairs DSBs in the absence of a template and leads to alterations in the repaired DNA. However, NHEJ is functional in all phases of the cell cycle and is believed to participate in the repair of over 80% of DSBs induced by ionizing radiation (IR) in cancer cells (5).

DNA-dependent protein kinase (DNA-PK) is a serine/threonine kinase and a key driver of NHEJ repair, working in co-ordination with five additional factors, Ku70, Ku80, XRCC4, ligase IV, and Artemis (6). A heterodimer consisting of Ku70 and

Ku80 binds specifically to DSBs, recruits and activates the catalytic subunit DNA-PKc, which in turn recruits the XRCC4/ligase IV heterodimer responsible for resealing the break. Trimming of the DSB ends may require Artemis and other DNA polymerases specialized in repair-mediated DNA polymerization. The activation of DNA-PK through autophosphorylation is essential for proper execution of the repair process (7,8).

DNA-PK-knockout mice are viable, suggesting that pharmacological inhibition will not affect essential functions in mammalian organisms and may be tolerated for the duration of standard cancer therapy regimens (9,10). Several lines of experimental evidence suggest that inhibition of DNA-PK activity can effectively sensitize cancer cells to exogenous DSB DNA damage, such as IR and certain types of DSB-inducing chemotherapies (11-17). These conclusions are derived from experiments using molecular biology approaches (RNAi) to suppress DNA-PK expression or early chemical inhibitors as laboratory tools in cultured cancer cells. However, most of those tool compounds lacked the specificity and pharmacological properties needed to establish a proof of principle for selective DNA-PK inhibition as a therapeutic approach in relevant in vivo models.

Here, we describe M3814, a novel potent and selective pharmacological DNA-PK inhibitor. We show that M3814 effectively suppresses DSB repair in cancer cells in a DNA-PK-dependent manner and strongly potentiates the antitumor effect of IR and DSB-inducing chemotherapy in vitro and in vivo. Clinically relevant 6-week studies using fractionated radiation and M3814 in two human xenograft models demonstrated complete and durable tumor regression, providing a strong rationale for clinical testing.

Methods

Cell lines and reagents

M3814 (MSC2490484A) was synthesized in the department of Medicinal Chemistry at Merck KGaA, Darmstadt (18). Cell lines were obtained commercially (ATCC, Virginia, USA; ECACC, Salisbury, UK; JCRB, Ibaraki, Japan; RIKEN, Tsukuba, Japan) and cultured in medium recommended or previously tested for these cells (A549, BxPC-3, FaDu, HT-29: DMEM/10% FCS/10% CO_2; Calu-6: DMEM/10% FBS/NEAA/10% CO_2; Capan-1: DMEM/15% FBS/10% CO_2; DU-145: MEM alpha/10% FBS/2 mM glutamine/5% CO_2; EBC-1; MEM Eagle/10% FBS/2 mM glutamine/5% CO_2; HCT-116: MEM alpha/10% FBS/10% CO_2; KP-4: DMEM/Hams F12 1:1/10% FCS/2 mM glutamine/5% CO_2; MiaPaCa-2: DMEM/10% FBS/2.5% HS/10% CO_2; MO59K, MO59K: DMEM/Nut Mix F12/10% FBS/2.5 mM glutamine/NEAA/5% CO_2; A375, NCI-H460: RPMI 1640/2 mM glutamine/1 mM sodium pyruvate/5% CO_2). Short tandem repeat analysis was performed to confirm cell line identity. Mycoplasma infection was excluded using a PCR-based method. The rabbit monoclonal antibody EM09912 was generated at Epitomics Inc. (Burlingame, California). In brief, rabbits were immunized with KLH-coupled phosphopeptide (YSYSpSQDPRPA). Supernatants from hybridoma cells were tested for differential activity against the phospho- versus nonphosphopeptide using enzyme-linked immunosorbent assays (ELISAs) and subsequently verified by western blotting. The antibody was purified from hybridoma supernatant using a protein A affinity chromatography.

Protein kinase assays

DNA-PK enzymatic assays were performed at concentrations of ATP near the Km (10 µM) or at 1 mM for time-resolved fluorescence energy transfer (TR-FRET). DNA-

PK purified from HeLa nuclear extracts was pre-incubated with M3814 at different concentrations (4.0E-15–3.0E-5 M) or vehicle for 15 minutes at 22°C in assay buffer. The reaction was started by addition of biotinylated STK-substrate (61ST1BLC, Cisbio), Mg-ATP, calf thymus DNA, and staurosporine, followed by incubation for 60–80 minutes at 22°C. The reaction was stopped with EDTA, and phospho-STK was detected with an anti-phospho-STK antibody (61PSTKLB, Cisbio) labeled with Europium as the donor, and streptavidin-labeled with XL665 (610SAXAC, Cisbio) as the FRET acceptor. Following incubation for 60 minutes, plates were analyzed on a Rubystar (BMG Labtech) microplate reader (excitation wavelength: 337 nm; emission wavelengths: 665 and 615 nm).

Ataxia telangiectasia-mutated (ATM) and ATM and rad3-related (ATR)/ATR-interacting protein (ATRIP) assays were performed using TR-FRET. Human recombinant ATM (14-933, Eurofins) or ATR/ATRIP (14-953, Eurofins) were pre-incubated in assay buffer for 15 minutes at 22°C with different concentrations of M3814 (4.0E-15–3.0E-5 M) or vehicle. The assay was started by addition of purified c-myc-tagged p53 (23-034, Eurofins) and ATP, and then incubated for approximately 30 minutes at 22°C. Reactions were subsequently stopped and antibodies were added (anti-phospho-p53(Ser15)-Eu [61P08KAY, Cisbio]; anti-cmyc [61MYCDAB, Cisbio]). After incubation for 2 hours, plates were analyzed in an EnVision (PerkinElmer) microplate reader (excitation at 340 nm, emission: 665 and 615 nm). Data were normalized to a DMSO control, and IC_{50} values were determined by non-linear regression analysis.

Protein and lipid kinase profiling was performed at Merck Millipore, Dundee, UK. Recombinantly produced protein and lipid kinases were used in enzyme activity assays. Protein kinase reactions were initiated with Mg-ATP and stopped after 40

minutes by addition of phosphoric acid. The transfer of radiolabeled γ-phosphate to peptide substrates was quantified by scintillation counting of peptide substrates immobilized on filter membranes. A non-radioactive assay (homogeneous time resolved fluorescence [HTRF]) was used for lipid kinases. The "percent of effect" activity was determined compared with vehicle-treated controls corrected for background activity. M3814 was tested at 1 µM (some cases 10 µM) or serially diluted for IC_{50} determination.

Western blot analysis

Exponentially growing HCT-116 and FaDu cancer cell lines were seeded in 12-well plates. The next day, the medium was removed, and cells were incubated with fresh medium containing a serial dilution of M3814 (concentration range: 1.5E-09–2.5E-05 M) and 10 µM bleomycin (for detection of phosphorylated DNA-PK) or 3 mM hydroxyurea (for detection of phosphorylated CHK1) for 6 hours. Cells were washed and lysed using HGNT buffer. After sodium dodecyl sulfate-polyacrylamide gel electrophoresis (SDS-PAGE), proteins were transferred to nitrocellulose membranes and incubated with primary antibodies (1:2000 anti-total DNA-PK, ab70250, Abcam; 1:1000 anti-pSer2056 DNA-PK, ab18192, Abcam; 1:1000 anti-pSer345 CHK1,2348, Cell Signaling; 1:200 anti-total CHK1sc8408, Santa Cruz) overnight at 4°C. Membranes were incubated with horseradish peroxidase (HRP)-conjugated secondary antibodies and developed using Lumi-Light^{PLUS} (Roche). Luminescence was recorded using a VersaDoc luminescent imager (Bio-Rad, Munich, Germany). pDNA-PK and pCHK1 values were normalized to total protein, and the bleomycin/hydroxyurea and DMSO controls were set to 0 and −100, respectively. Concentration-response curves were fitted using a nonlinear regression method to determine IC_{50} values. The experiment was repeated at least twice.

Immunofluorescence studies

A375 cells were seeded on eight-well glass chamber slides pre-coated with fibronectin. After 48 hours, the medium was removed and fresh medium without serum was added. The next day, the medium was removed and fresh medium with and without 1 µM M3814 was added 30 minutes prior to IR (2.4 Gy); the cells were further incubated for 0.5, 2, 4, 6, 8, or 24 h. Cells were fixed with methanol and stained with primary antibodies against phospho-histone H2A.X (1:8000 dilution, γH2A.X Ser139; clone 20E3; Cell Signaling 9718) overnight at 4°C, and subsequently with Alexa Fluor-conjugated secondary antibodies (1:2000 dilution, anti-rabbit IgG; Invitrogen A-11008). Immunofluorescence was determined at 40X magnification, γH2A.X foci were counted in 50–80 nuclei, and the numbers of cells with more than 10 γH2A.X foci per nucleus were counted and expressed as a percentage of total nuclei.

Immunohistochemistry

FaDu xenograft tumors were fixed in 4% buffered formaldehyde and embedded in paraffin. Sections (3 µm) were deparaffinized and heated to 96–100°C for epitope retrieval. Sections were incubated with primary antibodies (10 µg/mL anti-murine CD31, clone SZ31, DIA-310, Dianova; 1:50 anti-human γH2A.X, clone 20E3, 9718, NEB), and subsequently with Alexa Fluor-conjugated secondary antibodies (1:250 anti-rat IgG AF488: A-21208, Invitrogen; 1:250 anti-rabbit IgG AF594: A-11037, Invitrogen). Immunofluorescence was imaged at 40X magnification and the γH2A.X area inside nuclei (AF594 positive)/area nucleus (DAPI positive) was quantified. Data from vehicle- and drug-treated animals were compared by one-way ANOVA (Kruskal–Wallis test) followed by Dunn's Multiple Comparison Test (two-sided,

GraphPad Prism). Data are presented as the mean ± standard error of the mean (SEM).

Colony formation assay (CFA)

Cell survival was tested in response to IR at doses of 2.4 and 4.8 Gy using a Faxitron RX-650 irradiation device (Tucson, Arizona). Exponentially growing cancer cells (for cell lines see Table 2 and Fig. 1D) were seeded on six-well plates. Twenty-four hours later, cells were treated with a serial dilution of M3814 (typical concentration range: 2 x 10^{-9}–5 x 10^{-5} M) for 1 hour prior to radiation. After an additional 24 hours in the presence of M3814, the medium was substituted with fresh culture medium without compound. Cells were incubated for several days to weeks until visible colonies could be detected. Colonies were stained with neutral red or crystal violet and quantified using a Gelcount Scanner (Oxford Optronix, UK, England). Inhibition under each condition (single concentration and IR dose) was determined in singlicate in at least three independent experiments. Raw data were normalized by setting the cell number under DMSO treatment without IR to 100%. Concentration-response curves were fitted using a nonlinear regression method to determine IC_{50} values.

ELISA assays

Autophosphorylation of DNA-PK on serine 2056 was assessed by ELISA with a pDNA-PK antibody (0.125 µg/mL, EM9912), a DNA-PK antibody (0.5 µg/mL, WH0005591M2) for capture, and a biotinylated DNA-PK antibody (0.15 µg/mL, Abcam, ab79444) for detection. The PathScan Phospho-Chk2 (Thr68) Kit (Cell Signaling) was used according to the manufacturer's instructions to determine CHK2 phosphorylation on threonine 68. Exponentially growing cancer cells were treated with a serial dilution of M3814 (3E-10–3E-05 M) and 10 µM bleomycin for 6 hours. Cell lysates prepared in HGNT buffer were incubated with a solid phase-bound

capture antibody and further processed with a detection antibody and reagents. Phospho-DNA-PK and total DNA-PK chemiluminescence was quantified with a Mithras LB940 reader (Berthold, Bad Wildbad, Germany). The absorbance signal for phospho-CHK2 was measured at 450 nm using a Sunrise reader (Tecan, Männedorf, Switzerland). Phospho-DNA-PK values were normalized to total DNA-PK values; the bleomycin and DMSO controls were set to 0 and −100, respectively. For the PathScan Phospho-Chk2 (Thr68) Kit (Cell Signaling), background-corrected values were analyzed by setting the mean value of bleomycin-treated controls to 0% and transforming the absorbance values measured for the compound-treated samples to percentages. IC_{50} values were calculated by non-linear regression. Each experiment was repeated at least three times.

Cancer cell line profiling in combination with IR or other drugs

Radiosensitization of 92 cancer cell lines and resting peripheral blood mononuclear cells (PBMCs) by M3814 was performed at Oncolead (Karlsfeld, Germany). Cell viability was determined with 3 Gy IR (Cobalt-60 source), M3814 (5 µM–5 nM), and a combination of 3 Gy IR and M3814 (5 µM–5 nM). Treated cells were incubated for 120 hours, fixed, stained with sulforhodamine B, and quantified colorimetrically (18). EC_{50} (half-maximal effective concentrations) values were calculated from the concentration response data. Because 50% inhibition of viability was not observed in a substantial proportion of cell lines, EC_{50} data were displayed and analyzed.

Drug combination profiling of M3814 with 72 antitumor agents was performed in 34 cancer cell lines at Oncolead (Karlsfeld, Germany). Cell viability was determined with 72 drugs in concentration response, M3814 at a fixed concentration of 0.3 µM, and a combination of both. After 120-hour incubation, cells were fixed, stained with sulforhodamine B, and quantified colorimetrically (19). Bliss independence was used

to calculate synergy (20). In brief, the Bliss independence method compares the observed effect size $E_{measured}$ of a drug combination with the calculated effect, with E_{calc} assuming complete independence of the drug effects ($E_{calc} = E_{Drug1} + E_{Drug2} – E_{Drug1}E_{Drug2}$). Calculated Bliss values represent the mean values from all concentration combinations of a specific drug combination (synergy >0.1; 0.1≥ additivity ≥-0.1; antagonism <-0.1).

In vivo efficacy and pharmacokinetic (PK)/pharmacodynamic (PD) studies

In vivo efficacy data were generated in squamous cell head and neck FaDu (ATCC®, HTB-43™) and non-small cell lung cancer (ATCC®, HTB-177™) NCI-H460 human xenograft models in mice. The study designs and animal usage were approved by local animal welfare authorities (Regierungspräsidium Darmstadt, Hesse, Germany, protocol registration numbers DA4/Anz.397 and DA4/Anz.398). Seven- to nine-week-old female NMRI (nu/nu) mice were used (Charles River Laboratories, Sulzfeld, Germany). Mice received subcutaneous injections in the right thigh with 2.5 million FaDu or NCI-H460 cells. When tumor xenografts reached a mean volume of 50–115 mm^3, mice (n=10 per treatment arm, randomized from 15 mice per arm to obtain a similar mean and median within the treatment groups) received IR (2 Gy, X-RAD320 irradiation cabinet, Precision X-ray Inc.; settings: 10 mA, 250 kV, 58 s, 50 cm FSD collimator, 2 mm A1 filter). Mice were irradiated in groups of 10 and were anaesthetized during the irradiation process. IR was administered locally by positioning the tumor-bearing part of the leg in the beam path while shielding other body parts of the mice with lead. M3814 was formulated in vehicle (0.5% Methocel, 0.25% Tween20, 300 mM Sodium Citrate buffer pH 2.5) and administered orally at different doses, or in combination with IR for 5 days/week for 1 or 6 weeks. Mice were irradiated 10 minutes after oral administration of M3814. Tumor length (L) and

290 width (W) were measured with calipers and tumor volumes were calculated using
291 L×W^2/2.

292 Pharmacodynamic (PD) data were generated in FaDu human xenograft models in
293 mice. M3814 was administered orally once (5, 25, or 100 mg/kg) in combination with
294 10 Gy IR. Animals were sacrificed at different time points (0.16, 1.5, 3, 8, or 24 hours)
295 and tumors were removed, frozen in liquid nitrogen, lysed with HGNT buffer, and
296 homogenized using a Precellys-24 homogenizer. Cell lysates were transferred to
297 capture antibody-coated (mouse anti-DNA-PK 1B9, Abnova H00005591-M02, 2
298 µg/mL for coating) microtiter plates (Mesoscale, L15XB-6) and detected with either
299 total DNA-PK (mouse anti-DNA PK biotin 3H6; Cell Signaling, 12311BF, 0.1 µg/mL
300 followed by a secondary streptavidin Sulfo-TAG antibody, 0.2 µg/mL; Mesoscale,
301 R32AD-1) or phospho-DNA-PK antibodies (rabbit anti-phospho-DNA PK MKV-2;
302 Epitomics/Abcam, MKV-2-99-12 used at 0.01 µg/mL followed by secondary anti-
303 rabbit sulfo-TAG antibody; Mesoscale 0.1 µg/mL, R32AB-1). Plates were analyzed
304 using an MSD Sector imager 6000 (Model 1200).

305 Whole blood from healthy donors (N=6) was treated with M3814 (concentration
306 range: 1.0E-09–3.E-05 M) and bleomycin (100 µM) for 4 hours at 37°C. PBMCs were
307 isolated by density gradient separation with Leucosep filled tubes (VWR GREI
308 227288) and lysed using HGNT buffer. Cell lysates were transferred to capture
309 antibody-coated (2 and 4 µg/mL mouse anti- DNA PK; Sigma Aldrich
310 WH0005591M2) microtiter plates (Mesoscale; L15XB-6) and detected with either
311 total DNA-PK (1 µg/mL mouse anti-DNA PK; Abcam ab79444; followed by a 1 µg/mL
312 secondary streptavidin Sulfo-TAG antibody; Mesoscale; R32AD-1) or phospho-DNA-
313 PK (0.1 µg/mL rabbit anti-phospho-DNA PK MKV-2; Epitomics/Abcam; MKV-2-99-12

314 followed by a 1 µg/mL secondary anti-rabbit sulfo-TAG antibody; Mesoscale; R32AB-
315 1) antibodies. Plates were read using an MSD Sector imager 6000 (Model 1200).

316

Results

M3814 is a potent and selective inhibitor of DNA-PK activity

M3814 (MSC2490484A) is the product of a drug discovery screening and optimization program performed at Merck KGaA, Darmstadt, Germany. The structure of M3814 is shown in Fig. 1A and its synthesis described (18). Key pharmacological properties of M3814 are summarized in Table 1. M3814 inhibits DNA-PK activity with 0.6 nM IC_{50}) at an ATP concentration close to Km (10 μM). At a high ATP concentration (1 mM), the potency was reduced more than 30-fold, suggesting that M3814 competes with ATP for binding to DNA-PK.

M3814 exhibited a high degree of selectivity when tested using a broad panel of serine/threonine, tyrosine, and lipid kinases (Table 1). Only eight of 284 recombinantly expressed protein/lipid kinases, including mutant kinases, were inhibited by at least 50% at 1 μM M3814. All represented wild-type isoforms or mutant versions of lipid kinases of the PI3K family (Supplementary Table S1). PI3K kinases, ATM, ATR, mammalian target of rapamycin (mTOR), and DNA-PK, are members of the PI3K-related kinase family, which is characterized by high similarity in the kinase domain (21). Despite their high similarity, PI3K lipid kinase isoforms were affected with strongly reduced potency (>100-fold split). Other family members, ATR, ATM, and mTOR, were even less sensitive to M3814 (Table 1).

M3814 selectively inhibits DNA-PK activity and DSB repair in human cancer cell lines

M3814 inhibited DNA-PK autophosphorylation on Ser2056, a marker for DNA-PK activity in bleomycin-treated cancer cells, determined by western blot (Fig. 1B) or ELISA (Table 2). In bleomycin-treated HCT-116 cells, M3814 did not inhibit phosphorylation of the ATM kinase substrate CHK2 (Table 1). In contrast, a

moderate and concentration-dependent increase in CHK2 phosphorylation was observed, suggesting that DNA-PK blockade may trigger a compensatory upregulation of DSB repair (22). Hydroxyurea-induced CHK1 phosphorylation is induced by activation of ATR. M3814 did not block CHK1 phosphorylation, suggesting that ATR is not inhibited in cells. Phosphorylation of AKT on serine 473 in PC3 prostate cancer cells is driven by inactivation of phosphatase and tensin homolog (PTEN) and generation of phosphatidylinositol-3,4,5-triphosphate (PIP3) by PI3K activity (23). M3814 only moderately inhibited the phosphorylation of AKT, which is consistent with its weak inhibitory activity on the PI3K isoforms.

The reduced level of DNA-PK autophosphorylation by M3814 suggests that DNA-PK-dependent DSB repair by NHEJ is inhibited in cancer cells. To monitor the DSB level and repair kinetics in cancer cells, γH2AX-foci were counted at different time points after IR (Fig. 1C). Thirty minutes after IR, the number of cells with more than 10 foci increased and subsequently returned to baseline at 24 hours. Upon addition of M3814 (1 uM), the reduced number of foci over the recovery period was significantly inhibited compared with the DMSO-treated control, indicating that DNA-PK inhibition effectively suppressed DSB repair.

M3814 sensitizes cancer cells to IR

M3814 reduced colony formation in combination with IR in a concentration-dependent manner but showed no or limited activity in the absence of IR (Fig. 1D, Table 2). Overall, the antitumor potency correlated well with the inhibition of DNA-PK autophosphorylation, indicating that DNA-PK inhibition sensitizes cells to IR. The ability of M3814 to inhibit DNA-PK autophosphorylation and reduce colony formation was observed in all cancer cell lines tested, regardless of tumor origin. However, level of inhibition varied depending on the cancer cell line (Table 2). The antitumor

effect of M3814 was due to suppressing DNA-PK catalytic activity; in the glioblastoma cell line, MO59J, which lacks DNA-PK activity (24), increasing concentrations of M3814 did not further enhance sensitization to IR (Table 2, Fig. 1E). However, the DNA-PK-proficient cell line, MO59K, isolated from the same tumor specimen, was less sensitive to IR alone but was sensitized by M3814 in a concentration-dependent manner, suggesting that pharmacological inhibition of DNA-PK is the key mechanism of radiosensitization. Enhancement factors at 10% colony survival (EF10) for M3814 reached values between 2.5 and 6 in the 0.11–1 µM concentration range.

Suppression of colony formation is a widely used test to assess radiosensitization. However, its application is limited because many cancer cell lines do not form countable colonies (25). To assess M3814 activity in combination with IR in a large panel of cancer cell lines, we used a sulforhodamine B-based cell growth/viability assay. A random collection of 92 cancer cell lines, representing multiple tumor types, was used in the assay. M3814 inhibited cell growth with a mean EC_{50} of 2.1 µM (Fig. 2A, Supplementary Table S2). The effect on growth/viability in the absence of IR was more pronounced than in the colony formation assay, probably due to extended exposure to the compound. Nevertheless, the potency of inhibition by M3814 alone was regarded as rather moderate. In combination with 3 Gy IR, synergistic growth inhibition was observed in all cell lines, with a mean 12.4-fold EC_{50} shift in sensitization (Mean $EC50_{[M3814+IR]}$ = 0,17 µM; Supplementary Table S2, Supplementary Fig. S1). Taken together, our data suggest that by inhibiting DNA-PK activity and DSB repair, M3814 sensitizes cancer cells to IR through impaired colony outgrowth or proliferation/viability.

M3814 synergistically enhances the activity of DSB-inducing agents

To investigate the combination potential of M3814 with other anticancer agents, 35 randomly selected cancer cell lines were profiled with 72 drugs, representing diverse antitumor mechanisms of action. The inhibitory effect of each agent was measured in the presence or absence of 300 nM M3814 and Bliss synergy was calculated (20). Bliss scores were classified as synergistic (>0.1), additive (–0.1≤X≤0.1), or antagonistic (<-0.1; Fig. 2B, Supplementary Fig. S2). No significant combination effect was observed with the majority of tested drugs in most cancer cell lines, indicating that M3814 does not broadly synergize with anticancer agents. Notably, M3814 synergy across different cell lines was observed with the radiomimetic drug, bleomycin, and the topoisomerase inhibitors, doxorubicin and etoposide. These agents induce DSBs via radical generation or topoisomerase 2 inhibition, indicating that DNA-PK is important for repair of these lesions. Although sporadic synergism or antagonism was observed in a few individual cell lines, implying that the genetic make-up of the cancer cell lines may contribute to the combination effect, the overall ability of M3814 to synergistically enhance the activity of other drugs was clearly defined by their mechanism of action. Only three out of 72 drugs showed significant synergism in 34 cancer cell lines; those drugs are known to induce DSBs. These results clearly indicated that M3814 activity is derived from its molecular mechanism of action.

M3814 inhibits radiation-induced DNA-PK autophosphorylation and DSB repair in tumor xenograft models

Next, we asked whether M3814 could inhibit its target and the repair of IR-induced DSBs in tumor tissues in vivo. We performed PK/PD analyses in tumor xenograft studies. Initial results indicated that detection of DNA-PK autophosphorylation at low IR doses of 1–5 Gy is technically difficult and would not allow accurate quantification,

while a higher IR dose (10 Gy) resulted in a detectable increase of pSer2056 in DNA-PK, which returned to baseline levels over 24 hours (Fig. 3A). Following oral administration of a single dose of 25 mg/kg M3814, the plasma concentration of the parent compound increased to approximately 3 µM 1.5-hours post-dose, followed by elimination over the next 24 hours. IR-induced Ser2056 phosphorylation of DNA-PK was suppressed at 1.5 hours to below baseline levels and remained low 3 hours after IR. The signal increased at 8 hours, when the plasma concentrations of M3814 were lower, and returned to baseline levels at 24 hours. Autophosphorylation of DNA-PK was reduced in a concentration-dependent manner at 1.5 hours (Fig. 3B).

To assess the effect of DNA-PK inhibition on DSB repair, we developed an immunofluorescence-based assay for quantification of γH2A.X foci in tumor tissue (Fig. 3C, see methods), which was used to measure γH2A.X levels in FaDu tumors. A single dose of IR (10 Gy) was given in the presence or absence of M3814 (200 mg/kg) and γH2A.X signals were quantified in xenograft tumors obtained at different intervals post-IR. M3814 administration changed the kinetics of the γH2A.X signal compared with vehicle-treated tumors, indicating suppression of DSB repair (Fig. 3C, D). Taken together, these results indicate that M3814 administration inhibited IR-induced DNA-PK activation, leading to increased DSB levels, both consistent with the exposure dynamics of M3814 in mouse plasma.

Preincubation of human blood with M3814 attenuates DNA-PK phosphorylation

Pharmacodynamic (PD) data obtained from human tumor biopsies helps to confirm the drug reaches its molecular target in the target tissue. However, the possibility to sample tumor tissue in early clinical trials is rather low, making it difficult to build a robust PK/PD model. Analyses of PD biomarkers from surrogate tissues, such as

blood, offer the possibility for regular sampling in parallel to routine PK analyses. For this purpose, we developed a PD biomarker assay to detect DNA-PK autophosphorylation in peripheral blood cells. DNA-PK phosphorylation was induced by incubation of PBMCs from healthy human donors with bleomycin for 4 hours (Fig. 3E). Preincubation of human blood with different concentrations of M3814 ranging from 1 nM to 30 µM attenuated DNA-PK phosphorylation in a concentration-dependent manner. The potency of inhibition was within the same range observed for cancer cell lines. These data demonstrated that PD analyses from surrogate tissue are feasible and may be useful for clinical exploration of M3814.

M3814 strongly potentiates IR efficacy in xenograft models of human cancer

M3814 demonstrated good oral bioavailability and PK in mice (Supplementary Table S3, Supplementary Fig. S3); thus, further studies were performed to assess antitumor activity and evaluate safety in mouse xenograft models. Subcutaneously established FaDu or NCI-H460 tumors were treated with a 5-day fractionated radiation regimen (2 Gy IR fraction per tumor/mouse per day), with or without M3814 administered by oral gavage 10 minutes before IR. In both tumor models, tumor growth was moderately but significantly retarded with IR alone (Fig. 4A, B). However, co-administration of M3814 led to enhanced tumor growth inhibition in both tumor models. Tumor growth inhibition was dependent on the dose of M3814 administered (Fig. 4A). Additional human xenograft models of different origin were investigated (A549, BxPC3, Capan-1, and HCT-116) using the same IR regimen. Again, significant tumor growth inhibition was seen when M3814 was combined with IR for 1 week (Supplementary Fig. S4). NHEJ repair is independent of the cell cycle phase, fast, and contributes to the repair of most DSB lesions during the first hours after radiation (26). Indeed, the results of scheduling experiments of M3814 in relation to

IR support this hypothesis (Supplementary Fig. S5). When M3814 was administered 10 minutes prior to IR, the combination benefit was clearly superior than when administered 3 or 6 hours after IR. Since M3814 is rapidly cleared in mice, administration of an additional, consecutive dose of M3814 (first dose 10 minutes before IR, second dose 3-hours later) also improved antitumor activity. However, administration of M3814 for additional days after IR did not further improve antitumor efficacy indicating that DSBs have already been repaired.

In clinical practice, fractionated radiation regimens are commonly used for the treatment of multiple solid tumor types. The duration of radiation therapy with curative intent usually extends several weeks of therapy and applies fractionated doses of 1.8–2.0 Gy, for a total dose of approximately 50–70 Gy, depending on the tumor type and location (27). Therefore, we applied a 6-week radiotherapy regimen (5 days on, 2 days off) with 2 Gy fractions to subcutaneously implanted mouse xenograft tumors and investigated the effect of different doses of M3814 together with IR (Fig. 4C, D, Supplementary Fig. S6). In the FaDu head and neck cancer model, IR led to a partial regression of tumors during the treatment phase (Days 1–42); however, tumor growth progressed upon cessation of IR (Fig. 4C). With increasing doses of M3814 administered orally 10 minutes before each IR fraction, the tumor response was significantly enhanced, with increased tumor growth retardation at 5 and 10 mg/kg and complete regression of all tumors observed at 25 and 50 mg/kg doses. Of note, the strong response to combination therapy extended beyond treatment throughout the observation period (Days 43–106). Since the FaDu model is sensitive to IR alone (28), we assessed the impact of combination therapy in the relatively radio-resistant non-small cell lung cancer model, NCI-H460 (Fig. 4D). Indeed, this model was significantly less responsive to IR alone compared with FaDu tumors. During the

treatment period, H460 xenografts continued to grow following treatment with IR alone. However, co-administration of M3814 and IR significantly increased the antitumor response during the treatment and observation period. In five of 10 animals treated with 25 mg/kg M3814 plus IR, tumors progressed during the observation period (Days 49–97). Conversely, durable tumor responses were observed in the other five mice, and in all 10 mice treated with 50 mg/kg M3814 plus IR.

In general, the combination of M3814 plus IR was well-tolerated (Supplementary Fig. S6). During the treatment period, animals in all treatment groups showed a moderate loss of body weight (less than 10%), likely due to the daily (5 days on, 2 days off) treatment procedure, including anesthesia, oral gavage, and IR over 6 weeks. However, the body weight loss was fully reversible, and mice recovered during the observation period. In the FaDu efficacy study, grade 1 acute dermatitis was observed in only three out of 10 mice in the combination group receiving 50 mg/kg M3814 after 42 days of treatment; however, this was fully reversible after 14 days. No signs of dermatitis were observed in the other groups (29).

Applying clinically relevant IR treatment regimens to human tumor models in mice confirmed the remarkable antitumor activity of M3814 in combination with IR, which warrants clinical exploration.

Discussion

M3814 is a potent inhibitor of DNA-PK catalytic activity with remarkable selectivity against most of the 284 protein kinases we tested, including the closest members of its own kinase family. Cell-based experiments indicated that the in vitro selectivity is retained in cancer cells, albeit with reduced potency due to high ATP concentrations and possibly other factors, such as the nuclear localization of the target. Neither the ATR-CHK1 nor ATM-CHK2 pathways were significantly inhibited by M3814 in cancer cells at concentrations that effectively suppressed the DNA-PK pathway. Residual inhibitory activity against three closely related lipid kinases, PI3K$\alpha/\beta/\delta$, has been noted. However, phosphorylation of AKT in PTEN-mutated prostate carcinoma cells, which can be potently blocked by PI3K inhibitors, was only marginally inhibited.

M3814 inhibited DSB repair and sensitized cancer cells to IR. Treatment of cancer cells with M3814 attenuated foci resolution, indicating inhibition of DSB repair. Radio-sensitization was observed in most tested cancer cell lines, regardless of tissue origin, and confirmed using two different assay formats. The level of synergy varied moderately between cancer cell lines, suggesting that other factors have a subtle influence on sensitivity to the combination treatment. However, as expected, there was a good correlation between sensitivity to IR alone and to combination treatment with M3814. This suggests that the DNA-PK inhibitor enhances existing sensitivity to radiation rather than engaging a different antitumor mechanism. Strikingly, the glioblastoma line MO59J, which is devoid of DNA-PK activity (24), could not be radiosensitized by M3814, whereas the DNA-PK-proficient cell line, MO59K, which originates from the same tumor specimen, was sensitive to M3814. These data indicate that inhibition of DNA-PK kinase activity is the key mechanism underlying radiosensitization by M3814. Taken together, our results suggest that inhibition of the

canonical NHEJ pathway is responsible for the strong antitumor effects of M3814 when combined with IR.

Profiling M3814 in combination with 72 diverse established and developmental antitumor agents revealed potential for combination with the chemotherapeutics bleomycin, etoposide, and doxorubicin. These synergistic combinations were anticipated based on their mechanisms of action, which involve the generation of DSBs through inhibition of the topoisomerase enzymatic cycle leading to the generation of Top2:DNA complexes. DNA-modifying agents (alkylators, antimetabolites, and topoisomerase 1 inhibitors) did not synergize with M3814, since their primary mechanism of repair does not require the canonical NHEJ. Similarly, multiple other mechanisms represented by the large panel of tested drugs do not provide combination benefit, further indicating that M3814 acts exclusively by inhibiting NHEJ.

Exposure-dependent inhibition of DNA-PK autophosphorylation, and the subsequent delay in DSB repair kinetics observed in xenograft tissues in vivo, indicated that M3814 possesses all the necessary properties to evaluate the therapeutic potential of DNA-PK inhibition in xenograft models. To this aim, we selected two xenograft tumor models with different sensitivity to IR and the most relevant clinically established regimen for radiation therapy; 6-week fractionated radiation dosing. Pilot 1-week fractionated radiation studies showed that the combination of M3814 and IR is beneficial over IR alone. However, the 6-week animal trials, which modeled a clinically relevant fractionated radiation regimen with curative intent, demonstrated strong and durable antitumor activity of the M3814/IR combination. Local tumor radiation with M3814 exposures predicted to be achievable in man caused durable tumor regression in multiple animals in both models. In general, M3814 was well-

559 tolerated with moderate but completely reversible body weight loss. In one xenograft
560 study grade 1 radiation-induced dermatitis was observed in three out of ten animals
561 receiving the highest dose of M3814 (50 mg/kg) in combination; however, the
562 symptoms were fully reversible. Lower M3814 doses, which also produced complete
563 regressions, did not lead to a skin reaction. However, the limited toxicological data
564 presented here do not sufficiently address the impact of M3814 on other normal
565 tissues in the radiation field, especially toxic effects that manifest themselves
566 significantly later post-radiation treatment. Further combination studies with M3814
567 and dedicated toxicological assessments will help to better evaluate radiation-related
568 toxicities.

569 Data on the discovery and characterization of a novel DNA-PK inhibitor, M3814
570 presented in this manuscript offer a basis to explore its activity in combination with
571 radiotherapy and other DSB-inducing therapies in the clinic. Furthermore, the data
572 provide preclinical proof of concept for selective pharmacological inhibitors of DNA-
573 PK as combination partners of clinically established regimens for radiation therapy.
574 Currently ongoing clinical investigations with M3814 in both monotherapy and
575 radiotherapy combination settings should answer many outstanding questions
576 regarding their therapeutic potential (NCT02316197, NCT02516813).

577 **Acknowledgments:**

578 We would like to thank Isabella Schmele, Nina Heiss, Jesse Alderson, and Florian
579 Szardenings for their help in the preparation of this manuscript. Editorial assistance
580 was provided by David Lester and Lisa Jolly, PhD, of Bioscript Science, Macclesfield,
581 UK, and funded by Merck KGaA, Darmstadt, Germany.

582 **Authors contributions:**

583 **Conception and design:**

584 F.T. Zenke, A. Zimmermann, C. Sirrenberg, H. Dahmen, V. Kirkin, U. Pehl, T.
585 Grombacher, L. Vassilev, C. Wilm, T.

586 **Development of methodology:**

587 F.T. Zenke, A. Zimmermann, C. Sirrenberg, H. Dahmen, V. Kirkin, U. Pehl, T.
588 Grombacher, C. Wilm, T.

589 **Acquisition of data (provided animals, acquired and managed patients,**
590 **provided facilities, etc.):**

591 F.T. Zenke, A. Zimmermann, C. Sirrenberg, H. Dahmen, V. Kirkin, U. Pehl, C. Wilm

592 **Analysis and interpretation of data (e.g., statistical analysis, biostatistics,**
593 **computational analysis):**

594 F.T. Zenke, A. Zimmermann, C. Sirrenberg, H. Dahmen, V. Kirkin, U. Pehl, T.
595 Grombacher, C. Wilm, T., L. Vassilev

596 **Writing, review, and/or revision of the manuscript:**

597 F.T. Zenke, A. Zimmermann, C. Sirrenberg, H. Dahmen, V. Kirkin, U. Pehl, T.
598 Grombacher, C. Wilm, T. Fuchss, C. Amendt, L. Vassilev, A. Blaukat

599 **Administrative, technical, or material support (i.e., reporting or organizing data,**
600 **constructing databases):**

601 F.T. Zenke, A. Zimmermann, C. Sirrenberg, H. Dahmen, U. Pehl, T. Grombacher, C.
602 Wilm, C. Amendt, L. Vassilev

603 **Study supervision:**

604 F.T. Zenke, A. Zimmermann, C. Sirrenberg, H. Dahmen, V. Kirkin, U. Pehl, C. Wilm,

605 **Other (compound design and synthesis):**

606 T. Fuchss

References

1. Hanahan D, Weinberg RA. Hallmarks of cancer: the next generation. Cell **2011**;144(5):646-74 doi 10.1016/j.cell.2011.02.013.
2. Desai A, Yan Y, Gerson SL. Advances in therapeutic targeting of the DNA damage response in cancer. DNA Repair (Amst) **2018**;66-67:24-9 doi 10.1016/j.dnarep.2018.04.004.
3. Chapman JR, Taylor MR, Boulton SJ. Playing the end game: DNA double-strand break repair pathway choice. Mol Cell **2012**;47(4):497-510 doi 10.1016/j.molcel.2012.07.029.
4. Kasparek TR, Humphrey TC. DNA double-strand break repair pathways, chromosomal rearrangements and cancer. Semin Cell Dev Biol **2011**;22(8):886-97 doi 10.1016/j.semcdb.2011.10.007.
5. Kakarougkas A, Jeggo PA. DNA DSB repair pathway choice: an orchestrated handover mechanism. Br J Radiol **2014**;87(1035):20130685 doi 10.1259/bjr.20130685.
6. Davis AJ, Chen BP, Chen DJ. DNA-PK: a dynamic enzyme in a versatile DSB repair pathway. DNA Repair (Amst) **2014**;17:21-9 doi 10.1016/j.dnarep.2014.02.020.
7. Salles B, Calsou P, Frit P, Muller C. The DNA repair complex DNA-PK, a pharmacological target in cancer chemotherapy and radiotherapy. Pathol Biol (Paris) **2006**;54(4):185-93 doi 10.1016/j.patbio.2006.01.012.
8. Dobbs TA, Tainer JA, Lees-Miller SP. A structural model for regulation of NHEJ by DNA-PKcs autophosphorylation. DNA Repair (Amst) **2010**;9(12):1307-14 doi 10.1016/j.dnarep.2010.09.019.
9. Taccioli GE, Amatucci AG, Beamish HJ, Gell D, Xiang XH, Torres Arzayus MI*, et al.* Targeted disruption of the catalytic subunit of the DNA-PK gene in mice confers severe combined immunodeficiency and radiosensitivity. Immunity **1998**;9(3):355-66.
10. Kurimasa A, Ouyang H, Dong LJ, Wang S, Li X, Cordon-Cardo C*, et al.* Catalytic subunit of DNA-dependent protein kinase: impact on lymphocyte development and tumorigenesis. Proc Natl Acad Sci U S A **1999**;96(4):1403-8.
11. Azad A, Jackson S, Cullinane C, Natoli A, Neilsen PM, Callen DF*, et al.* Inhibition of DNA-dependent protein kinase induces accelerated senescence in irradiated human cancer cells. Mol Cancer Res **2011**;9(12):1696-707 doi 10.1158/1541-7786.MCR-11-0312.
12. Block WD, Merkle D, Meek K, Lees-Miller SP. Selective inhibition of the DNA-dependent protein kinase (DNA-PK) by the radiosensitizing agent caffeine. Nucleic Acids Res **2004**;32(6):1967-72 doi 10.1093/nar/gkh508.
13. Daido S, Yamamoto A, Fujiwara K, Sawaya R, Kondo S, Kondo Y. Inhibition of the DNA-dependent protein kinase catalytic subunit radiosensitizes malignant glioma cells by inducing autophagy. Cancer Res **2005**;65(10):4368-75 doi 10.1158/0008-5472.CAN-04-4202.
14. Hashimoto M, Rao S, Tokuno O, Yamamoto K, Takata M, Takeda S*, et al.* DNA-PK: the major target for wortmannin-mediated radiosensitization by the inhibition of DSB repair via NHEJ pathway. J Radiat Res **2003**;44(2):151-9.
15. Munck JM, Batey MA, Zhao Y, Jenkins H, Richardson CJ, Cano C*, et al.* Chemosensitization of cancer cells by KU-0060648, a dual inhibitor of DNA-PK and PI-3K. Mol Cancer Ther **2012**;11(8):1789-98 doi 10.1158/1535-7163.MCT-11-0535.
16. Dong J, Ren Y, Zhang T, Wang Z, Ling CC, Li GC*, et al.* Inactivation of DNA-PK by knockdown DNA-PKcs or NU7441 impairs non-homologous end-joining of radiation-induced double strand break repair. Oncol Rep **2018**;39(3):912-20 doi 10.3892/or.2018.6217.
17. Zhuang W, Li B, Long L, Chen L, Huang Q, Liang ZQ. Knockdown of the DNA-dependent protein kinase catalytic subunit radiosensitizes glioma-initiating cells by inducing autophagy. Brain Res **2011**;1371:7-15 doi 10.1016/j.brainres.2010.11.044.
18. Fuchss T, Emde U, Buchstaller H-P, Mederski WKR; Arylquinazolines 2014;Patent WO2014183850A1, example 136, (S)-[2-Chloro-4-fluoro-5-(7-morpholin-4-yl-quinazolin-4-yl)-phenyl]-(6-methoxy-pyridazin-3-yl)-methanol.

19. Vichai V, Kirtikara K. Sulforhodamine B colorimetric assay for cytotoxicity screening. Nat Protoc **2006**;1(3):1112-6 doi 10.1038/nprot.2006.179.
20. Berenbaum MC. What is synergy? Pharmacol Rev **1989**;41(2):93-141.
21. Lempiainen H, Halazonetis TD. Emerging common themes in regulation of PIKKs and PI3Ks. EMBO J **2009**;28(20):3067-73 doi 10.1038/emboj.2009.281.
22. Sun Q, Guo Y, Liu X, Czauderna F, Carr MI, Zenke FT*, et al.* Therapeutic implications of p53 status on cancer cell fate following exposure to ionizing radiation and the DNA-PK inhibitor M3814. Mol Cancer Res **2019** doi 10.1158/1541-7786.MCR-19-0362.
23. Sharrard RM, Maitland NJ. Regulation of protein kinase B activity by PTEN and SHIP2 in human prostate-derived cell lines. Cell Signal **2007**;19(1):129-38 doi 10.1016/j.cellsig.2006.05.029.
24. Hoppe BS, Jensen RB, Kirchgessner CU. Complementation of the radiosensitive M059J cell line. Radiat Res **2000**;153(2):125-30.
25. Franken NA, Rodermond HM, Stap J, Haveman J, van Bree C. Clonogenic assay of cells in vitro. Nat Protoc **2006**;1(5):2315-9 doi 10.1038/nprot.2006.339.
26. Lobrich M, Jeggo P. A Process of Resection-Dependent Nonhomologous End Joining Involving the Goddess Artemis. Trends Biochem Sci **2017**;42(9):690-701 doi 10.1016/j.tibs.2017.06.011.
27. Arnold KM, Flynn NJ, Raben A, Romak L, Yu Y, Dicker AP*, et al.* The Impact of Radiation on the Tumor Microenvironment: Effect of Dose and Fractionation Schedules. Cancer Growth Metastasis **2018**;11:1179064418761639 doi 10.1177/1179064418761639.
28. Kasten-Pisula U, Menegakis A, Brammer I, Borgmann K, Mansour WY, Degenhardt S*, et al.* The extreme radiosensitivity of the squamous cell carcinoma SKX is due to a defect in double-strand break repair. Radiother Oncol **2009**;90(2):257-64 doi 10.1016/j.radonc.2008.10.019.
29. Cox JD, Stetz J, Pajak TF. Toxicity criteria of the Radiation Therapy Oncology Group (RTOG) and the European Organization for Research and Treatment of Cancer (EORTC). Int J Radiat Oncol Biol Phys **1995**;31(5):1341-6 doi 10.1016/0360-3016(95)00060-C.

688 **Tables**

689 **Table 1:** M3814 potency and selectivity

Assay		IC_{50} [nM]
DNA-PK, IC_{50} [10 µM ATP]		0.6
DNA-PK, IC_{50} [1,000 µM ATP]		20
Protein Kinases Panel profiling		276/284 not inhibited ≥ 50% at 1µM
PIKK Family Members	ATM	10,000
	ATR	2,800
	hPI3Kalpha	330
	hPI3Kbeta	250
	hPI3Kgamma	>1,000
	hPI3Kdelta	95
	mTOR	>10,000
HU-induced pS345-CHK1		>25,000
Bleomycin-induced pT68-CHK2		>5,000
Constitutive pS473-AKT in PC3		3,800

690 ATM, ataxia telangiectasia-mutated; ATP, adenosine triphosphate; ATR, ATM and
691 rad3-related; CHK, checkpoint kinase; DNA-PK, DNA-dependent protein kinase; IC_{50},
692 half maximal inhibitory concentration; mTOR, mammalian target of rapamycin.

693

694

695 **Table 2:** Cellular profiling of M3814 in cancer cell lines

Cellular profiling of M3814					
Cancer cell line	Origin	Bleomycin-induced pDNA-PK, IC_{50} [M]	Clonogenicity ± irradiation, IC_{50} [M]		
			0 Gy	2.4 Gy	4.8 Gy
MO59J	Brain	n.d.	4×10^{-5}	No concentration-dependence	
MO59K	Brain	2×10^{-7}	1×10^{-5}	4×10^{-7}	3×10^{-7}
HCT-116	Colon	1×10^{-7}	$>1 \times 10^{-5}$	2×10^{-7}	8×10^{-8}
HT29	Colon	1×10^{-7}	2×10^{-5}	4×10^{-7}	2×10^{-7}
FaDu	Head and neck	6×10^{-8}	1×10^{-5}	1×10^{-7}	5×10^{-8}
A549	Lung	2×10^{-7}	1×10^{-5}	1×10^{-7}	5×10^{-8}
Calu-6	Lung	2×10^{-7}	1×10^{-5}	7×10^{-8}	3×10^{-8}
EBC-1	Lung	2×10^{-7}	1×10^{-5}	1×10^{-7}	5×10^{-8}
NCI-H460	Lung	1×10^{-6}	3×10^{-5}	2×10^{-7}	1×10^{-7}
BxPC-3	Pancreas	2×10^{-7}	1×10^{-5}	1×10^{-7}	7×10^{-8}
KP-4	Pancreas	4×10^{-7}	3×10^{-5}	2×10^{-7}	7×10^{-8}
MiaPaCa	Pancreas	5×10^{-7}	$> 5 \times 10^{-5}$	2×10^{-7}	9×10^{-8}
DU145	Prostate	3×10^{-7}	2×10^{-5}	3×10^{-7}	1×10^{-7}

696 DNA-PK, DNA-dependent protein kinase; Gy, Gray unit; IC_{50}, half maximal inhibitory
697 concentration.

698

Figure legends

Figure 1: M3814 in combination with IR inhibits DNA-PK activity and reduces cancer cell survival in a DNA-PK-dependent manner.

A) Chemical structure. **B)** Concentration-dependent inhibition of DNA-PK autophosphorylation by M3814 in bleomycin-treated cancer cell lines, HCT-116 and FaDu, as shown by western blotting. Total DNA-PK was used as a loading control. Representative images are shown. **C)** M3814 (1E-6 M) in combination with IR (2.4 Gy) suppressed DSB repair, as assessed by the number of γH2A.X foci in cells. A high basal level of γH2A.X foci was noted in A375 cells; therefore, the percentage of cells with >10 γH2A.X foci was calculated and the time course of foci dynamics is plotted (bottom). Representative immunofluorescent images of vehicle-treated A375 cells without IR (top image) and 30-minutes after IR (2.4 Gy) (bottom image) are shown. **D)** M3814 (4E-7 M, 2E-8 M) in combination with IR (2.4 Gy, 4.8 Gy) reduced colony formation in FaDu and HCT-116 cancer cells in a clonogenic cell survival assay. Visible colonies were stained with neutral red. Representative images of at least three assays are shown. **E)** M3814 in combination with IR reduced colony formation of glioblastoma cell lines in a DNA-PK-dependent manner. M3814 combined with IR had no effect on colony survival versus vehicle in the DNA-PK-deficient glioblastoma cell line, MO59J (top panel). With increasing concentrations of M3814 combined with IR, the surviving fraction of colonies was reduced versus vehicle in the DNA-PK-proficient glioblastoma cell line, MO59K (bottom panel).

Figure 2: In combination with IR, M3814 broadly reduces the viability of cancer cell lines and synergistically enhances the activity of DNA DSB-inducing drugs.

A) Sulforhodamine B-based cell growth/viability of 92 cancer cell lines in response to M3814 alone and in combination with IR (3 Gy). Calculated EC_{50} from M3814 (5E-9–5E-5 M) titrations alone (grey bars) or in combination with 3 Gy IR (red bars) are presented for all tested cell lines. Cell lines were sorted from low to high sensitivity to M3814 alone. Mean $EC50_{[M3814]}$ = 2.1 µM and mean $EC50_{[combination]}$ = 0,17 µM are displayed as lines. **B)** Heat map of Bliss synergy scores for combination profiling of 72 drugs, including DNA-damaging agents, tested in 34 cancer cell lines; synergistic (≥0.1; red), additive (–0.1<X<0.1; white), and antagonistic (≤-0.1; blue).

Figure 3: M3814 inhibits radiation-induced DNA-PK activation leading to increased DSB levels in tumor tissue from mice xenograft models; assessment of DNA-PK phosphorylation and inhibition by M3814 in human blood. A) Time course of DNA-PK phosphorylation in the FaDu tumor xenograft model in response to IR (10 Gy) alone (black line) or the combination of M3814 (25 mg/kg) with IR (10 Gy, red line). Data from a representative PK/PD study are shown. The ratio of phosphorylated to total DNA-PK was determined in five tumors per treatment group and time points, and the mean +/- SEM are presented. The mean plasma concentration of M3814 over time following oral administration is shown in green. **B)** The ratio of phosphorylated to total DNA-PK was determined in FaDu xenograft tumors at baseline (no IR), after 10 Gy IR alone, and following treatment with IR (10 Gy) combined with M3814 (5, 25, 100 mg/kg). Tumors were processed 1.5 hours after treatment (five tumors per group). **C)** Impaired DSB repair over time in FaDu tumors following treatment with vehicle (left image) or 200 mg/kg M3814 (right image) and IR (10 Gy). Representative immunofluorescence images detecting γH2A.X in tumor sections are shown (Scale bar = 2 µm). **D)** Quantification of time-dependent

resolution of γH2A.X staining from the experiment described under C. **E)** DNA-PK phosphorylation was induced by incubating whole blood from healthy donors with bleomycin for 4 hours (left). Preincubation of whole blood with M3814 attenuated bleomycin-induced DNA-PK phosphorylation in a concentration-dependent manner, confirming target modulation by M3814 in human blood samples. Representative data from a single donor are shown (blood from 6 different donors was tested).

Figure 4: M3814 in combination with IR has antitumor activity in mouse xenograft models. A) M3814 (oral gavage 10-minutes before IR; dose groups: 25, 100, 150 mg/kg) in combination with a 5-day fractionated radiation regime (2 Gy IR fraction/mouse per day) dose-dependently reduced tumor growth in a human FaDu xenograft model to a greater extent than IR alone. Data represent the mean +/- SEM (group size N=10). **B)** M3814 (oral gavage 10-minutes before IR; dose: 150 mg/kg) in combination with a 5-day fractionated radiation regime (2 Gy IR fraction/mouse per day) reduced tumor growth in a human NCI-H460 xenograft model. Data represent the mean +/- SEM (group size N=10). **C)** M3814 (5, 10, 25, 50 mg/kg) in combination with a 6-week radiotherapy regime (2 Gy fractions, 5 days on, 2 days off) demonstrated dose-dependent antitumor activity in a human FaDu xenograft model. Data represent the mean +/- SEM (group size N=10). **D)** M3814 (25 and 50 mg/kg) in combination with a 6-week radiotherapy regime (2 Gy fractions, 5 days on, 5 days off) demonstrated antitumor activity in a human radio-resistant NCI-H460 xenograft model (group size N=10).

Figure 1

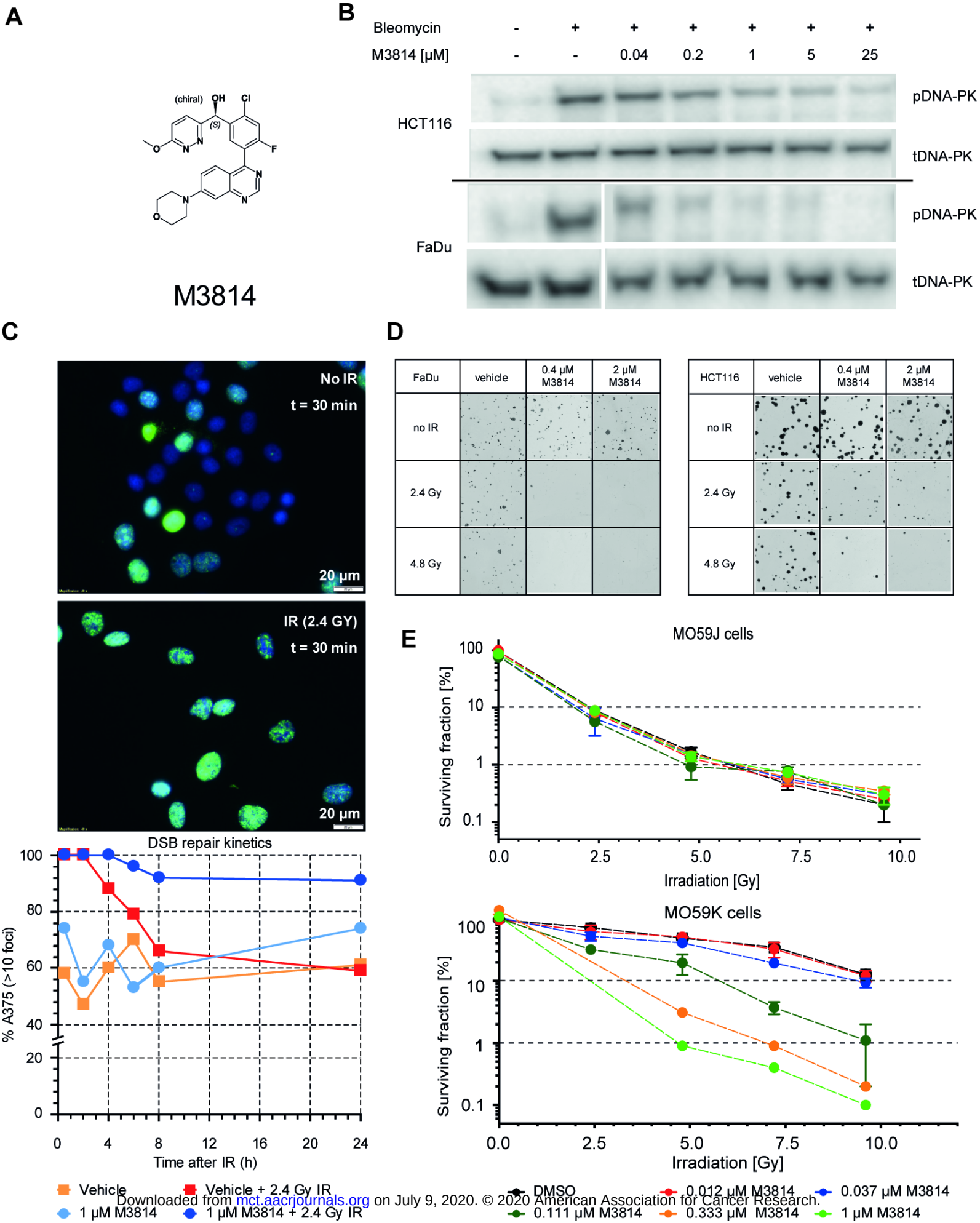

Figure 2

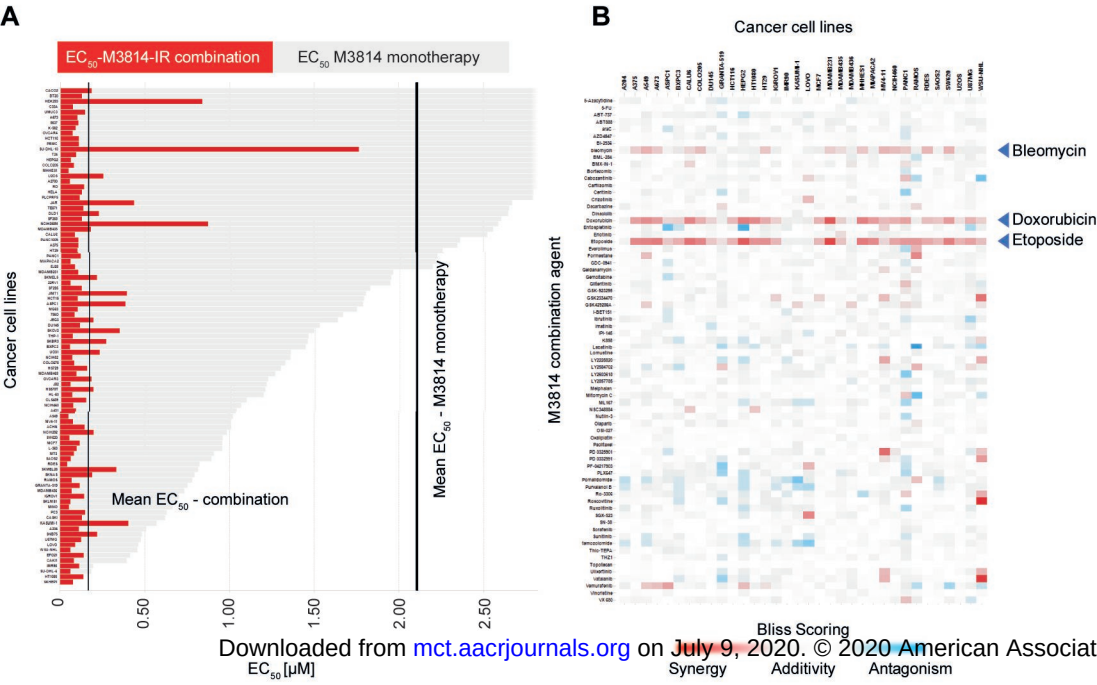

Figure 3

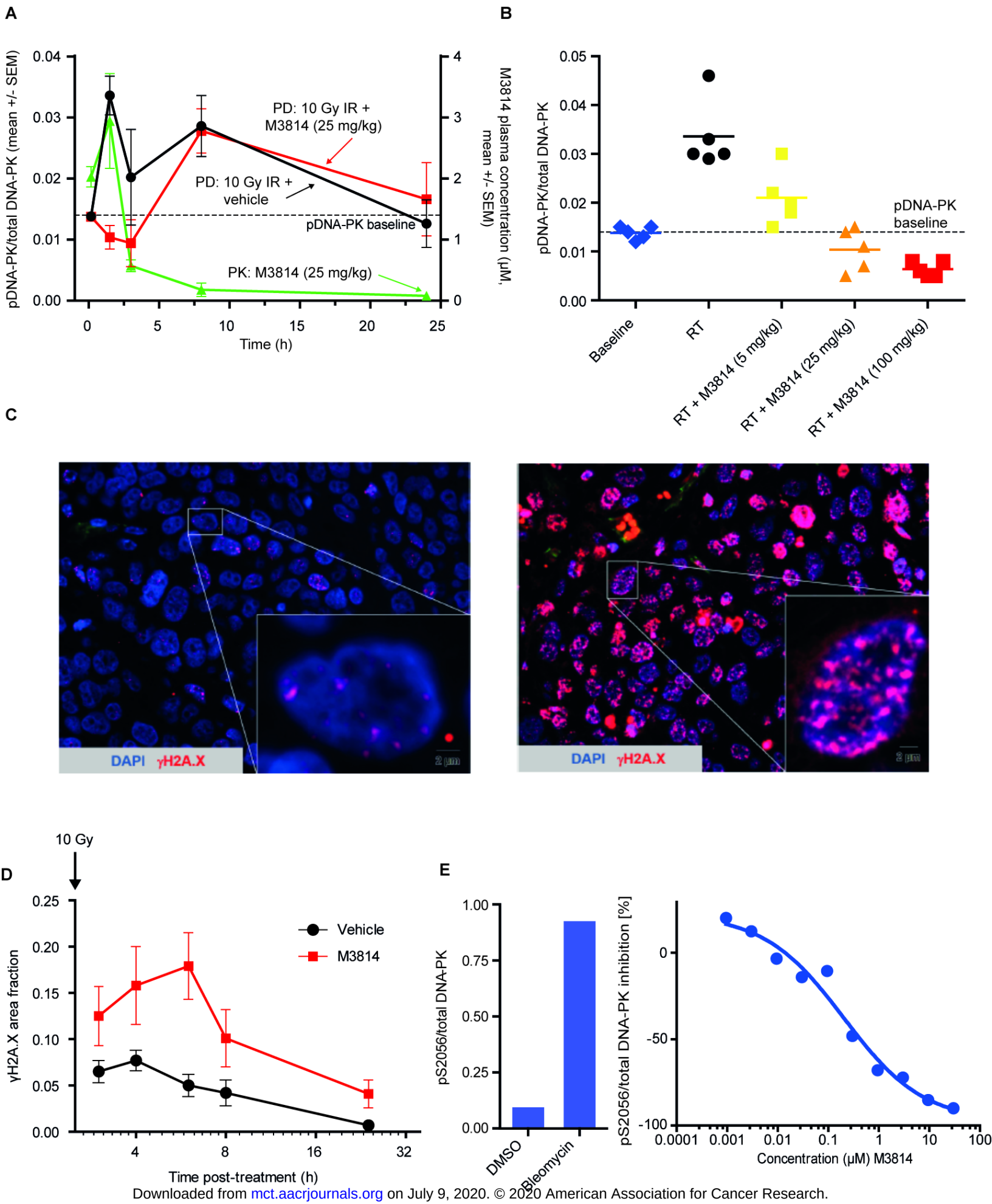

Figure 4

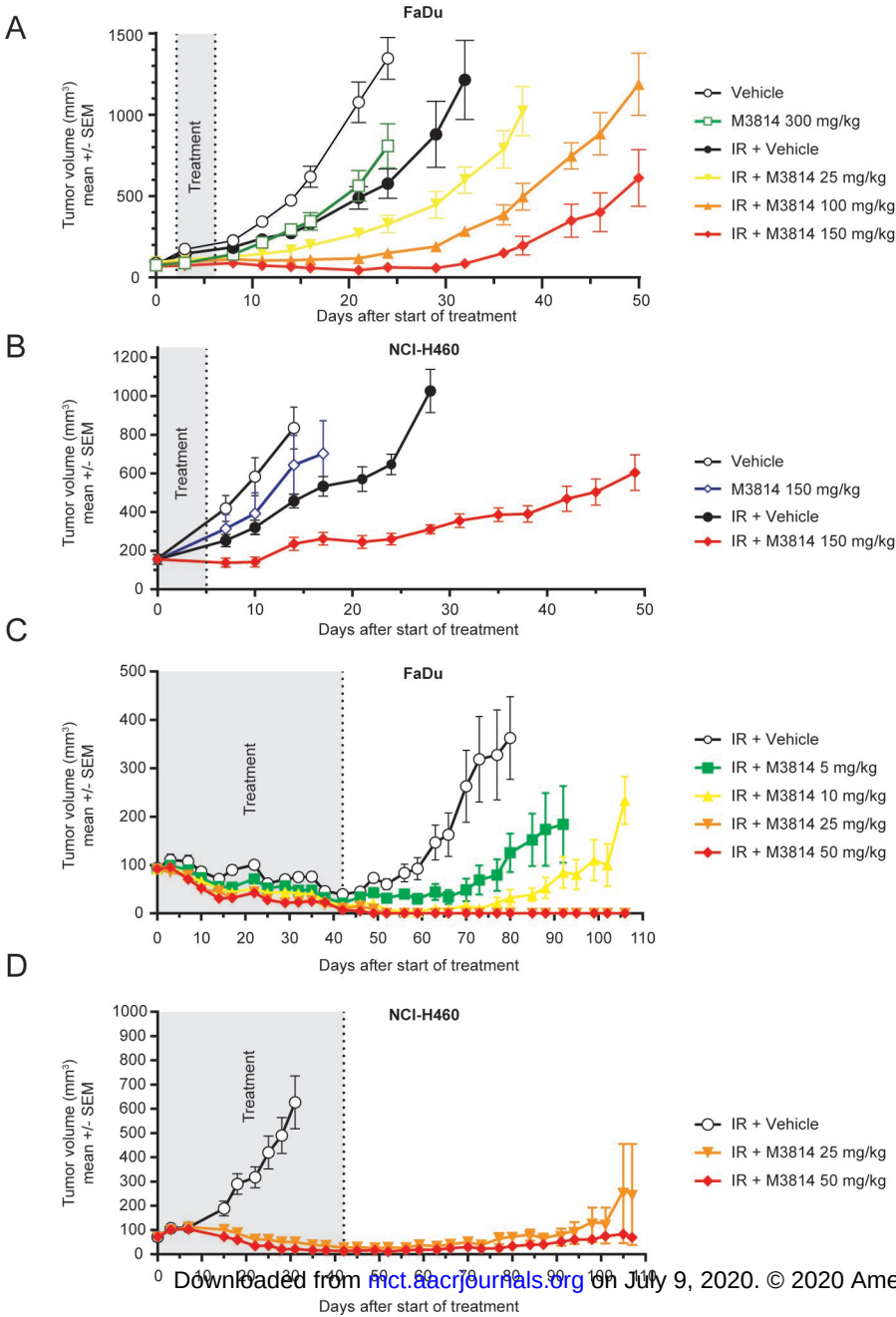

AACR American Association for Cancer Research

Molecular Cancer Therapeutics

Pharmacological inhibitor of DNA-PK, M3814, potentiates radiotherapy and regresses human tumors in mouse models

Frank T. Zenke, Astrid Zimmermann, Christian Sirrenberg, et al.

Mol Cancer Ther Published OnlineFirst March 27, 2020.